Composites Science and Technology 166 (2018) 160–168

Contents lists available at ScienceDirect

Composites Science and Technology

journal homepage: http://www.elsevier.com/locate/compscitech

Synergetic effects of thin plies and aligned carbon nanotube interlaminar reinforcement in composite laminates

Estelle Kalfon-Cohen [a, *], Reed Kopp [a], Carolina Furtado [a, c, d], Xinchen Ni [b], Albertino Arteiro [c], Gregor Borstnar [e], Mark N. Mavrogordato [e], Ian Sinclair [e], S. Mark Spearing [e], Pedro P. Camanho [c, d], Brian L. Wardle [a]

[a] Department of Aeronautics and Astronautics, Massachusetts Institute of Technology, 77 Massachusetts Avenue, Cambridge, MA, 02139, USA
[b] Department of Mechanical Engineering, Massachusetts Institute of Technology, 77 Massachusetts Avenue, Cambridge, MA, 02139, USA
[c] DEMec, Faculdade de Engenharia da Universidade do Porto, Rua Dr. Roberto Frias, s/n, 4200-465, Porto, Portugal
[d] INEGI, Instituto de Ciência e Inovação em Engenharia Mecânica e Engenharia Industrial, Rua Dr. Roberto Frias, 400, 4200-465, Porto, Portugal
[e] Faculty of Engineering and the Environment, University of Southampton, Highfield, Southampton, SO17 1BJ, UK

ARTICLE INFO

Article history:
Received 1 September 2017
Received in revised form
19 December 2017
Accepted 4 January 2018
Available online 9 January 2018

Keywords:
Thin-ply laminate
Carbon nanotube
Mechanical properties
Finite element analysis

ABSTRACT

Thin-ply carbon fiber laminates have exhibited superior mechanical properties, including higher initiation and ultimate strength, when compared to standard thickness plies and enable greater flexibility in laminate design. However, the increased ply count in thin-ply laminates also increases the number of ply-ply interfaces, thereby increasing the number of relatively weak and delamination-prone interlaminar regions. In this study, we report the first experimental realization of aligned carbon nanotube interlaminar reinforcement of thin-ply unidirectional prepreg-based carbon fiber laminates, in a hierarchical architecture termed 'nanostitching'. We synthesize a baseline effective standard thickness laminate using multiple thin-plies of the same orientation to create a ply block, and we find an ~15% improvement in the interlaminar shear strength via short beam shear (SBS) testing for thin-ply nanostitched samples when compared to the baseline. This demonstrates a synergetic strength effect of nanostitching (~5% increase) and thin-ply lamination (~10% increase). Synchrotron-based computed tomography of *post mortem* SBS specimens suggests a different damage trajectory and mode of damage accumulation in nanostitched thin-ply laminates, notably the complete suppression of delaminations in the nanostitched region. Finite element predictions of damage progression highlight the complementary nature of positive thin-ply and nanostitching effects that are consistent with an ~15% improvement in Modes I and II interlaminar fracture toughness due to the aligned carbon nanotubes at the thin-ply interfaces.

1. Introduction

Fiber-reinforced laminated composites are attractive for many applications, especially in the aerospace industry where high mechanical performance under extreme loading combined with low density is desired. Despite their general outstanding performance, such composites are well-known to be vulnerable to microscopic damage that accumulates under mechanical and thermal loading [1]. Although the failure behavior of laminated composites and their structures has been carefully studied, the mechanisms are difficult to predict accurately since they depend on many geometrical and structural properties, such as stacking sequence, material, ply thickness, component geometry, and loading conditions, among others [2,3]. Spread-tow thin-ply prepreg, herein called 'thinpreg', was introduced by Kawabe et al. [4–8], focuses on stable and gentle opening of dry tows so that even flatter fiber plies can be produced and subsequently pre-impregnated with a resin, as is commonly done for conventional thickness prepregs. This technique allows the production of ultra-thin prepreg (up to 7× thinner than traditional prepreg) while suppressing issues associated with fiber arrangement and ply uniformity. Thinpreg laminates have several considerable advantages in terms of design and mechanical performance such as the possibility of meeting design constraints with no change in laminate thickness and the use of smaller mismatch

* Corresponding author.
E-mail address: escohen@mit.edu (E. Kalfon-Cohen).

https://doi.org/10.1016/j.compscitech.2018.01.007
0266-3538/

angles that has been shown to improve the interfacial fracture resistance. It has also been shown that thin-ply laminated composites can suppress microcracking, delamination, and splitting damage [9–14]. This strengthening effect, which inhibits crack growth in off-axis plies within a laminate, is a consequence of the so-called "*in situ* effect", which is characterized by an increase in ply transverse and shear strengths when a ply is constrained by plies with different fiber orientations in a laminate [9]. In general, thin-ply composites exhibit enhanced unnotched and notched compressive strengths, better resistance to fatigue and, if designed to trigger specific damage mechanisms, enhanced notched tensile strength [9–14]. However, the use of thinpreg laminae presents an issue due to the larger number of assembly steps required to reach a desired laminate thickness, with the laminate then having a larger number of ply interfaces. The interlaminar region at each ply interface is comprised of pure (unreinforced) resin, as in any laminate, making it susceptible to interlaminar crack propagation and delamination and limiting the lifetime of the composite part [14]. While the prior work has indicated thin-ply laminates are less prone to delamination in comparison to standard thickness plies, the existence of additional delamination-prone regions is of concern for fatigue and damage tolerance. From the perspective of preventing early delamination and associated failure, reinforcing the interlaminar region has remained an active area of research for decades and includes technologies such as stitching, z-pinning, interleaving, and 3D weaving [15–22]. Thus, a drawback to thin-ply laminates is the increased number (and volume) of relatively weak interlaminar regions. Even though interlaminar stresses are reportedly lower in thin-ply laminates, delamination can still be an issue at the most critical interfaces, such as the inner interfaces in laminates subjected to large out-of-plane deformations. To achieve maximum delamination resistance, a combination of thin-plies and nanostructure reinforcement is proposed here.

In the past two decades, the use of nanomaterials as fillers and reinforcement in composites has emerged as a viable technique to increase the interlaminar toughness and strength without compromising the integrity of the microfiber laminate [23–26]. Recently, the ability to grow highly aligned arrays of densely packed carbon nanotubes (CNTs) offers the possibility of local reinforcement, due to the high mechanical properties of CNTs (*e.g.,* Young's modulus and strength equal to or exceeding aerospace-grade carbon fibers [18,27]) and developments in both fabrication and processing towards manufacturability [28]. Garcia et al. [29] introduced a hierarchical architecture where aligned CNTs (A-CNTs) are placed strategically between consecutive plies to reinforce the resin rich interlaminar region, termed 'nanostitching' that is utilized in the current work. This architecture was originally developed following fracture mechanics analysis that showed a strong scale effect between toughness and nanoscale fibers reinforcing cracks (Mode I analysis) [30]. In standard thickness laminates, prior work has shown that laminate-level in-plane strengths are increased, and damage propagation is delayed due to the presence of the stronger and tougher interlaminar region at all ply interfaces [30–32]. Notably, in-plane strengths were improved broadly and significantly: the critical bearing strength, the ultimate open-hole compression strength, and the L-shape laminate breaking energy of the nanostitched samples were increased by 30%, 14% and 40%, respectively, compared to the unreinforced samples [31].

Herein, A-CNT nanostitching is employed for the first time to reinforce the interlaminar region of thin-ply composite laminates. Nanostitched Thin, as well as an effective standard thickness (herein called 'Thick') version, quasi-isotropic (QI) symmetric laminates are fabricated and tested (see Fig. 1) in short beam shear (SBS) to focus on interlaminar failure. The effect of nanostitching thinpreg laminates is visualized using Synchrotron Radiation Computed Tomography (SRCT), which allows the non-destructive visualization and comparison of the internal damage extent of *post mortem* specimens. Damage trajectories and differences between the four tested laminate configurations are further analyzed by finite element simulations of progressive damage.

2. Methods

In the following sections, fabrication of the laminates is presented, including the A-CNT synthesis and transfer process, followed by the detailed experimental procedure for static SBS testing, characterization of *post mortem* samples, and detailed description of the finite element progressive damage modeling.

2.1. Materials and laminates fabrication

Vertically aligned CNTs were grown in a tube furnace (Lindberg/Blue M) by chemical vapor deposition (CVD) at atmospheric pressure following procedures previously documented [28]. The A-CNT forests have an areal density of ~1 vol% corresponding to 10^9-10^{10} CNTs per cm^2, and the CNTs are each comprised of 3–5 walls with an outer diameter of ~8 nm. The A-CNT forests are 20 ± 5 μm in height and are introduced into the interlaminar region by transferring them onto the surface of the composite prepreg plies before laminate assembly, making use of the tack of the prepreg at room temperature to adhere the forests to the prepreg plies. Details about the transfer process can be found in Ref. [29]. It is important to stress that the alignment of the A-CNT forests is preserved after transfer and no crushing is observed as seen in Fig. S1A (Supplementary Information), consistent with prior observations in related work [29,31]. A unidirectional aerospace-grade carbon fiber and epoxy thinpreg (Toho Tenax HTS40/Q-1112, 54 μm ply nominal thickness) was used for fabrication of the laminates. Two laminate types, Thin and Thick, were manufactured, with and without nanostitch, giving four laminate configurations in total. Thin consists of 48 thinpreg plies stacked in a quasi-isotropic (QI) symmetric layup $[(0/90/\pm45)_6]_s$, and Thick is an effective 16-ply $[(0_3/90_3/\pm45_3)_2]_s$ laminate fabricated by stacking three thinpreg plies (a ply block) with identical orientation to create an equivalent standard nominal ply thickness of 162 μm (see Fig. 1). Local nanostitching at the center of the laminate was utilized to reduce the amount of A-CNT material and the number of fabrication steps required and focused reinforcement on the center of the laminate for selective reinforcement based on reported modes of failure in the SBS ASTM standard [33]. A-CNT nanostitches were placed in the fifteen middle interfaces in the Thin laminate configuration, which is equivalent to five interfaces in the Thick laminate configuration, as displayed in Fig. 1. The effectiveness of the transfer process was visually evaluated to be ~90% by area. Each 30 cm × 30 cm laminated plate was identically packaged for autoclave curing, beginning with the arrangement of a sub-assembly from bottom to top with the following materials: flat aluminum mold plate with dimensions larger than the laminate, a layer of guaranteed non-porous Teflon (GNPT) covering the entire mold plate top surface, a layer of peel ply with dimensions slightly larger than the laminate, the composite laminate, and another layer of peel ply with dimensions slightly larger than the laminate. Next, a dam comprised of three layers of cork tape was placed snugly around the laminate perimeter and on top of both peel ply layers. Another layer of GNPT was draped over the cork dam. Then, a flat aluminum caul plate with dimensions identical to the laminate was pressed inside of the cork dam on top of the topmost GNPT layer, completing the sub-assembly. Next, the sub-assembly was wrapped in breather cloth, a vacuum port bottom-half was placed on top of the breather cloth over the mold plate, and the full assembly was inserted into

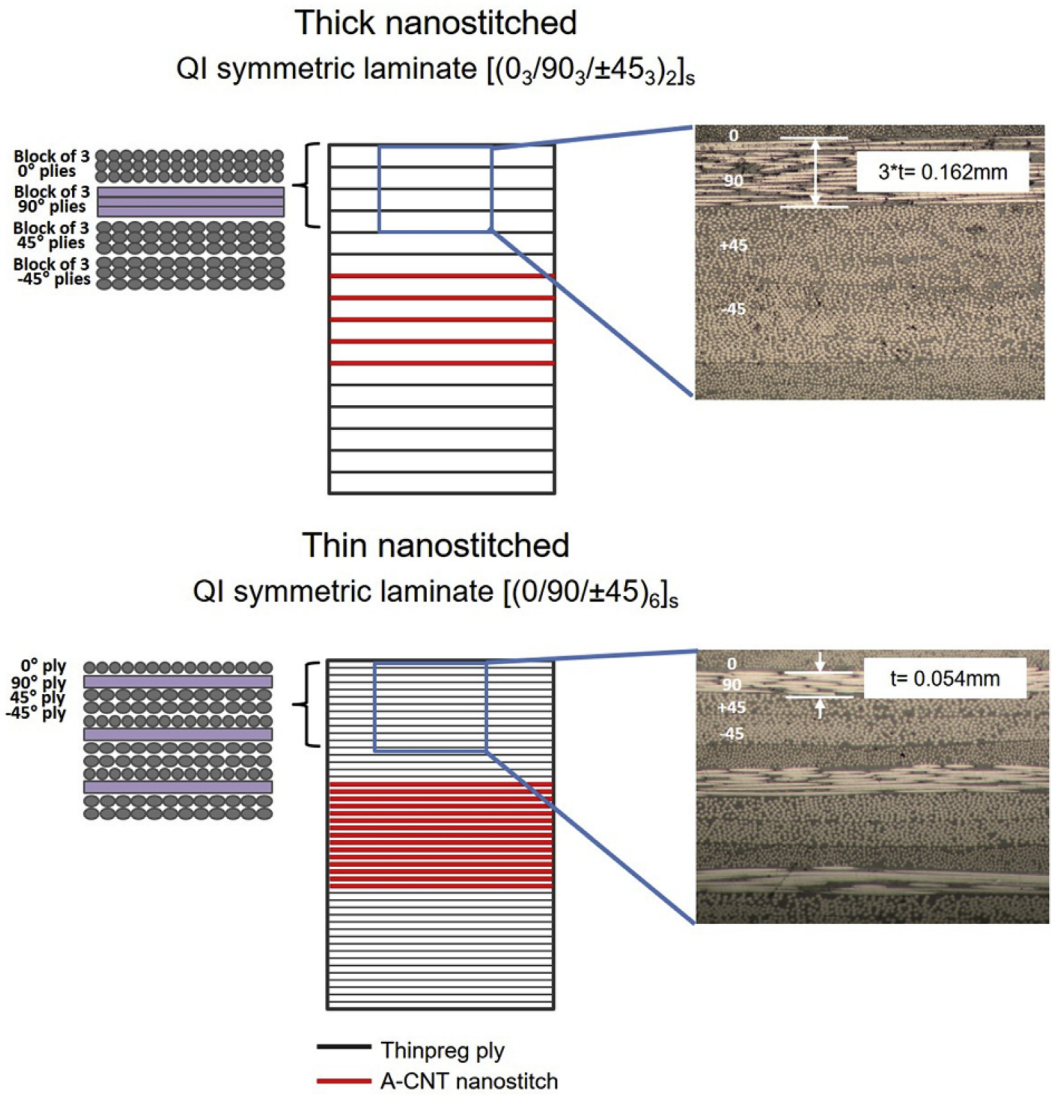

Fig. 1. Thick and Thin laminate configurations: (top) Illustration of Thick laminate consisting of the stacking of three consecutive thinpreg plies (black lines) to create an effective standard thickness laminate. The five midplane interfaces are nanostitched with A-CNTs (red) and a representative optical micrograph of a Thick cross-section appears at right. (bottom) Illustration of Thin laminate showing the fifteen midplane nanostitched interfaces (red) and a representative optical micrograph appears at right. In both cases the laminate layup is quasi-isotropic (QI). (For interpretation of the references to color in this figure legend, the reader is referred to the Web version of this article.)

vacuum bagging film that was sealed subsequently with sealant tape. Finally, a vacuum port top-half was joined to the bottom-half through a small incision created in the vacuum bag film.

The laminates were subsequently cured under vacuum in an autoclave following the manufacturer-specified cure procedure: 0 bar(g) of autoclave pressure at 2 °C/min to 80 °C, hold for 30 min, followed by 90 min at 130 °C and 6.9 bar(g) of autoclave pressure, cool at 3 °C/min to 60 °C and vent autoclave pressure, let cool to room temperature. In addition to the autoclave pressure, vacuum was applied at cure onset and until the autoclave pressure reached ~2 bar(g), at which point the vacuum was vented. Baseline and nanostitched specimens were taken from the same plate. Once the laminates were cured, specimens were cut to size and prepared for testing; specimen dimensions and test specifics are provided below.

2.2. Short beam shear strength testing

Procedures follow ASTM D2344 including laminate dimensions and polishing. The laminates were cut using a diamond-grit band saw into test coupons with dimensions of 5.2 mm × 15.6 mm × 2.6 mm for the width, length and thickness, respectively. The specimens were subsequently mechanically polished on the edges to remove defects introduced by the cutting process. The polishing process included sanding using 800-grit paper and polishing using 1 μm alumina powder. At least seven specimens of each configuration (Thick, Thick nanostitched, Thin, and Thin nanostitched) were tested under the static SBS configuration (ASTM D2344) [33]. The samples were loaded in a three-point configuration with a span of 10.5 mm at 1 mm/min. The load-displacement curves were recorded during testing until catastrophic failure, and interlaminar shear strength (ILSS) in SBS, σ_{SBS}, was calculated according to eq. (1):

$$\sigma_{SBS} = 0.75 \times \frac{P_{max}}{w \times t}, \tag{1}$$

where P_{max} is the maximum load and w and t are the width and the thickness of the specimen, respectively. After failure, all of the

samples were inspected under an optical microscope to assess damage instances and their locations.

2.3. Transfer assessment and morphology of the interlaminar region

Since the reinforcing effect is expected to be a consequence of the presence of the A-CNTs at the interfaces, assessment of the morphology of the interlaminar region is particularly important. Scanning electron microscopy (Zeiss, Ultra Plus) was used to assess the quality of the CNT nanostitching transfer and measure the interlaminar thickness. At least 20 interfaces were observed and measured for each laminate configuration. The average interlaminar thickness for baseline Thin and Thick was found to be ~4 μm. The addition of A-CNT nanostitching (20 μm tall A-CNTs forest) to the interlaminar region increases the interlaminar thickness by ~50% as shown in Table 1. This was not observed in prior nanostitching work for standard thickness laminae [30,32,34], and further investigations should be done to ensure minimum increase of the interlaminar region thickness. Although the interlaminar region increased in thickness where A-CNTs were integrated, the overall laminate thickness was not statistically significantly increased (see Table 1), such that the overall laminate microfiber volume fraction across all laminate configurations was not affected. As observed in prior work with standard thickness prepreg [31], the addition of a 20 μm tall A-CNT forest does not increase the interlaminar thickness concomitantly, *i.e.*, the average thickness is statistically unchanged at 10 μm. While the A-CNT transfer process has no effect on the alignment (and hence height) as shown in Fig. S1A, autoclave processing, likely pressure and vacuum, compress the A-CNTs to ~7–10 μm. Fig. 2 shows representative high-resolution cross-sectional images of a typical interface in Thin baseline (Fig. 2a) and Thin nanostitched samples (Fig. 2b and c). The micrographs reveal that the A-CNTs were effectively transferred onto the prepreg, properly filling the interlaminar resin rich area. Furthermore, the A-CNTs effectively bridge the two plies and penetrate into each ply through the first row of microfibers at the ply-ply interfaces. This morphology is essential to the toughening mechanism associated with nanostitching, which often includes CNT pullout and bridging [32,34]. Similar features are observed in nanostitched interfaces of Thick baseline specimens as seen in Fig. S1B (Supplementary Information).

2.4. Synchrotron Radiation Computed Tomography ex situ damage investigation

SRCT experiments were carried out at the ID 19 beamline at the European Synchrotron Radiation Facility (ESRF) in Grenoble, France to understand damage in failed SBS specimens. Two thick baseline and two Thin laminate coupons (baseline and nanostitched) previously tested under short beam shear configuration were scanned *ex situ* using a 20 keV X-ray energy beam with radiograph projections captured at an ~0.7 μm isotropic voxel size (1.4 mm × 1.4 mm field of view) and 50 ms exposure. The region of interest is scanned through the thickness at the center of the specimen. Analysis and segmentation of the 3D volumes were performed using Avizo (FEI) commercial software version 9.2. Damage was segmented via a region-growing algorithm that was constrained by a user-specified gray value threshold. The process of manually selecting voxels in known damage regions and using a region-growing algorithm to automatically select eligible neighboring voxels was repeated until all user-identified damage had been segmented within a single SRCT volume dataset. For consistency, the same threshold was adopted as a standard for damage segmentation in all SRCT volume images featuring identical prepreg constituent materials and captured with identical X-ray imaging parameters.

2.5. Progressive damage modeling

Simulation of the SBS test was performed to better understand reinforcement of the laminate interfaces with A-CNTs. Damage simulation in composite laminates requires the use of models that can capture both intralaminar (matrix cracking, fiber fracture, etc.) and interlaminar (here, delamination) damage. In this work, intralaminar damage was simulated using the continuum damage model proposed by Maimí et al. [35–37]. Delamination was simulated using the cohesive zone model implemented in ABAQUS [38]. For nanostitched interfaces, this is a simplification since these models were not developed to account for any inelastic deformation and fracture of nano-reinforced interfaces. The model was composed of: (i) two lower supports and a loading nose composed of C3D8r elastic elements and (ii) the laminate. One user defined material C3D8r finite element per ply was used to simulate intralaminar damage and the plies were connected by 10 μm thick COH3D8 cohesive elements as shown in Fig. S2 (Supplementary Information). The supports and loading nose were also simulated to avoid unrealistic damage development at the outer layers because their dimensions were not negligible compared to the dimensions of the specimens. A mesh of 0.25 mm × 0.25 mm × t mm (where t is the ply thickness: 54 μm for the Thin configurations and 162 μm for the Thick configurations) was used for the ply elements and 0.25 mm × 0.25 mm × 0.01 mm was used for the cohesive elements. The element size used for the supports and the loading nose was ~0.25 mm × 0.25 mm × 0.25 mm. The mesh and boundary conditions used are shown in Fig. S2.

Since most of the material properties needed to simulate intralaminar and interlaminar damage are unknown for the HTS40/Q-1112 carbon/epoxy material system, approximations were made based on previous work. Regarding the simulation of the material behavior at the ply level, the most relevant ply properties used are presented in Table S3A (Supplementary Information). Properties for the HTS40/Q-1112 material were utilized when available and other properties were taken from prior work and open literature utilizing common carbon/epoxy values or from Hexcel IM7/8552 (see discussion in Supplemental Information, as well as Tables S3A and S3B). Note that the in-plane shear, transverse tensile, and transverse compressive strengths were calculated as a function of the ply thickness and ply position in the laminate following Ref. [39]. In the simulations of the unreinforced samples, the fracture toughness of the elements in every interface was the same. However, in the case of nanostitched interfaces, previous studies link the improvement in ILSS [30,31] to a substantial increase in the interlaminar

Table 1
Laminate and interlaminar thicknesses.

Laminate configuration	Laminate thickness (mm)	Interlaminar thickness (μm)
Thick baseline	2.58 ± 0.02	3.5 ± 1.3
Thick nanostitched	2.58 ± 0.01	7.9 ± 1.8
Thin baseline	2.60 ± 0.01	4.2 ± 1.1
Thin nanostitched	2.62 ± 0.01	7.8 ± 1.4

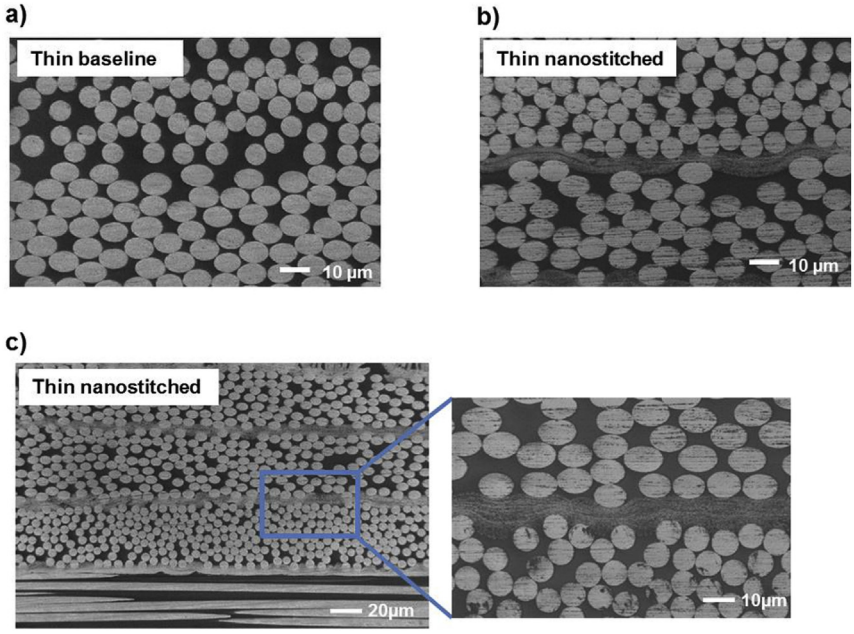

Fig. 2. Representative scanning electron micrographs of ply interfaces in baseline and nanostitched specimens: (a) a 90/45 interface in Thin baseline laminate, (b) a 90/45 interface in Thin nanostitched laminate. An A-CNT reinforced 90/45 interface with aligned CNTs visible as light grey area. (c) Lower magnification of 45/90/0 interfaces in Thin nanostitched laminate showing the A-CNTs bridging the layers of microfiber plies. On the right, a higher magnification of the Thin nanostitched 45/90 interface from (c).

toughness. Hence, in the present model, interlaminar elements representing nanostitched interfaces were parametrically given a higher fracture toughness (+5%, 10%, 15%, etc.) for which the baseline value was based on Hexcel IM7/8552 prepreg as a proxy material. The cohesive stresses were calculated using two engineering solutions proposed by Turon and co-authors [40,41] to enable a better representation of the softening behavior in the vicinity of the crack tip and to accurately calculate the energy dissipation. Damage propagation was associated with a damage variable, d, which was equal to 0 when the elements were undamaged and equal to 1 when the elements were fully damaged and are no longer able to carry load. In this work, only greatly damaged elements (with $d > 0.9$) and fully damaged elements (with $d = 1$) were highlighted to simplify the analysis. The detailed model, procedure, and results are presented and discussed in Sections S2 and S3 (Supplementary Information).

3. Results and discussion

The four specimen configurations were tested via SBS to measure the ILSS. This test type restricts the shear-dominated loading to a limited zone where relatively high interlaminar shear stresses develop, causing failure in an out-of-plane shear-dominated mode at the center of the laminate cross-section. Table 2 summarizes the ILSS results for the four laminate configurations, and representative load-displacement curves are shown in Fig. 3. Typical modes of failure observed include delamination at the center of the laminate cross-section and at the free edges along or near the laminate centerline but may also include fiber breaks and compressive damage at the load introduction points at the surface of the specimen, as identified in Ref. [33]. Within the Thick specimens, no statistically significant change was observed after nanostitching. This is in contrast to prior work that has shown a 6.5% increase in static SBS ILSS for standard thickness specimens of a different UD prepreg system (IM7/8552 by Hexcel) [32], although more recent work has also shown a statistically insignificant increase in static SBS ILSS, but a significant increase in fatigue life in SBS, for another UD standard thickness prepreg system (AS4/8552 by Hexcel) [42].

Table 2
Interlaminar Shear Strength (ILSS) via Short Beam Shear (SBS) for baseline and nanostitched Thick and Thin laminates. Only statistically significant changes are noted.

Laminate type	ILSS (MPa)	Change (% vs. Thick baseline)
Thick baseline	69.9 ± 2.4	
Thick nanostitched	69.8 ± 1.3	
Thin baseline	76.9 ± 1.1	+10.1%
Thin nanostitched	80.6 ± 0.6	+15.3%

It seems that small or negligible increases in strength are revealed in static SBS testing across the two standard thickness systems studied so far, similar geometrically to the blocked-ply Thick configuration herein. Furthermore, selective A-CNT nanostitching in only five interfaces is expected to have less effect than nanostitching in the full fifteen interfaces as in Ref. [33]. As noted earlier, future work will pursue optimizing the A-CNT forest height to maintain the interlaminar region thickness, as was achieved in the two prior standard thickness prepreg studies [31,32]. The comparison between Thin and Thick laminates shows an increase of 10% in the ILSS of Thin baseline over the Thick baseline samples and an additional 5% increase in the Thin nanostitched over the Thick baseline samples.

Visual inspection of *post mortem* specimens reveals that while multiple delaminations are observed in the midplane interfaces of the Thin baseline sample, 70% of Thin nanostitched specimens failed outside of the A-CNT reinforced areas. This was not observed in either Thick laminate configuration. These results support the hypothesis that nanostitching can delay ultimate failure, particularly in thinpreg laminates where the number of interfaces is increased relative to the equivalent Thick baseline. In Fig. 3, *post mortem* SEM observations of specimen cross-sections reveal extensive CNT pullout and local debonding of the CNT layer at the interlaminar region. This is expected since it was also reported in previous work on nanostitching [30–32] that delayed delamination

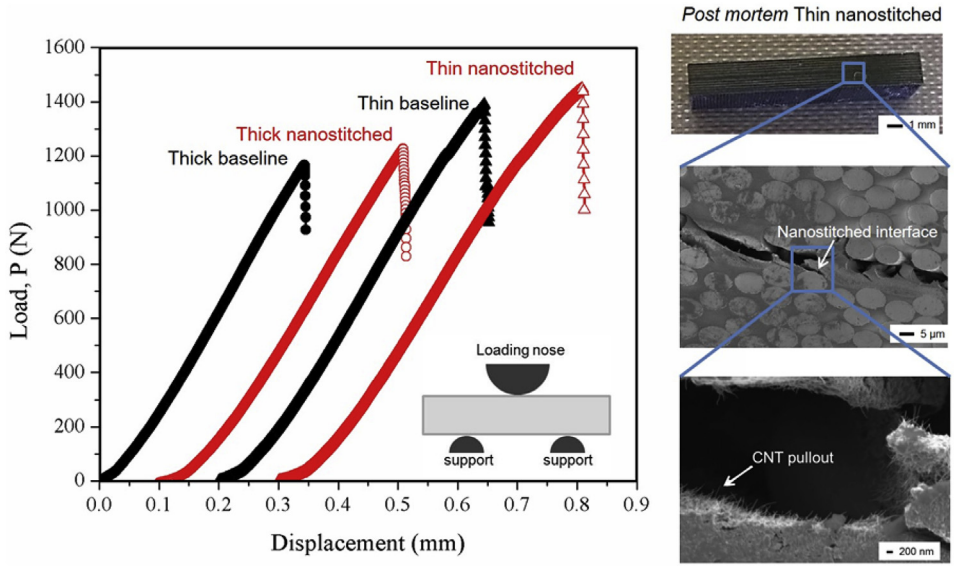

Fig. 3. Short beam shear strength (SBS) testing results: (left) Representative SBS load-displacement curves at the median values for interlaminar shear strength. For comparison, the curves were shifted along the x-axis. (right) Micrographs of a *post mortem* Thin nanostitched interface showing a crack through the nanostitch-ply interface and micrometer-long CNT pullout from the polymer.

is correlated to an increase in interlaminar fracture toughness, *i.e.*, reinforcement provided by the addition of high aspect ratio nanofibers (A-CNTs here).

To understand the mechanisms involved in the observed synergy between thin-ply technologies and A-CNT nanostitching, *post mortem* assessment of the damage type and extent was undertaken via computed tomography. Imaging a full volume in 3D was possible using SRCT, which allowed the visualization of internal damage with sufficient resolution to distinguish microfiber breaks, delamination, and intralaminar matrix cracks. *Post mortem* Thick (baseline), Thin and Thin nanostitched coupons were inspected by SRCT at ~ 0.7 μm isotropic voxel size. Since the effect of nanostitching was less pronounced in the Thick configuration, no SRCT analysis was performed on these samples. Damage, segmented in red for delamination and blue for matrix cracks, is shown in Fig. 4. Note that microfiber breaks exist, concentrated at the contact zone with the loading nose but are not shown in Fig. 4 since, qualitatively, no observable differences were discerned in the density or distribution of fiber breaks across any of the specimen configurations. The segmented damage reveals that Thick and Thin baselines fail differently. The Thick baseline sample contains extensive damage in the center of the specimen where shear stresses are highest in the SBS test, with large matrix cracks developing in the 45° plies and in the vicinity of clear inter-ply delamination planes. As expected, the Thin baseline sample exhibits more localized damage than the Thick baseline, with delaminations occurring at the 7th, 11th, and 29th interfaces and confined transverse matrix cracks developing in the 45° plies. The reason for the location of the delaminations is the high value of the transverse shear stress under the loading points as previously reported by Abali et al. [43]. This is one of several clear indications that the SBS test is more complex than a simple interlaminar shear strength test. We note the asymmetry of damage with respect to the specimen thickness in Fig. 4, particularly in the Thin specimens, i.e., more damage is evident under the loading nose which causes through-thickness compressive stress. As expected, the intralaminar cracks developed in the Thin baseline are arrested and remain constrained to the intralaminar regions, as opposed to the Thick baseline which exhibits intralaminar damage extending through consecutive thin-plies. This effect results in less extensive intralaminar damage that can be associated with higher strengths [44]. However, since the number of plies is effectively tripled and the number of interfaces is approximately tripled (47 vs. 15) in the case of thinpreg laminates, the number of delaminations is observed to increase similarly.

For Thick baseline samples, the matrix crack extension which occurs through the thickness of the three-ply block leads to ply stress relaxation, whereas in the Thin baseline, matrix cracks appear in individual thin-plies and arrest at interlaminar regions. It may be hypothesized that further increase of applied loading in Thin yields an increase in the matrix crack density within the laminae, introducing high stress fields at the interlaminar regions and consequently interlaminar damage, as seen in the high density of delamination zones in Fig. 4. Thin nanostitched samples exhibit similar intralaminar damage compared to Thin baselines in these *post mortem* investigations, indicating no obvious effect in this regard to the nanostitch. Although delaminations are still visible, the number of damaged interfaces is significantly reduced in the Thin ply nanostitched samples, and in the region that is reinforced with A-CNTs, delaminations are fully suppressed. The fact that no delamination is observed in the CNT area indicates a positive reinforcing effect. Although nanostitching yields only a 5% increase in the SBS ILSS for the Thin specimens, SRCT visualization demonstrates that delamination is clearly mitigated by nanostitching. Future work will need to reinforce all interfaces in the laminate with A-CNTs. Results of progressive damage modeling support the SRCT observations that the reinforcing effect of nanostitching for the Thin configuration has the clear effect of mitigating delaminations, and to a lesser extent, matrix cracking in the middle region of the laminate thickness as shown in Fig. 4. Damage accumulation at three points along the modeled load-deflection curve (not shown here) is reported for the three configurations in Fig. 5. Note that the matrix damage extent shown in the model results in Fig. 4 is different from the damage extent in Fig. 5, as the former (Fig. 4) looks at damage at the specimen surface, whereas the latter (Fig. 5) provides an integrated projection of all damage through the specimen width. The integrated view in Fig. 5 allows for a better comparison of damage extent for the different laminate configurations. In both figures, only damaged elements where the damage

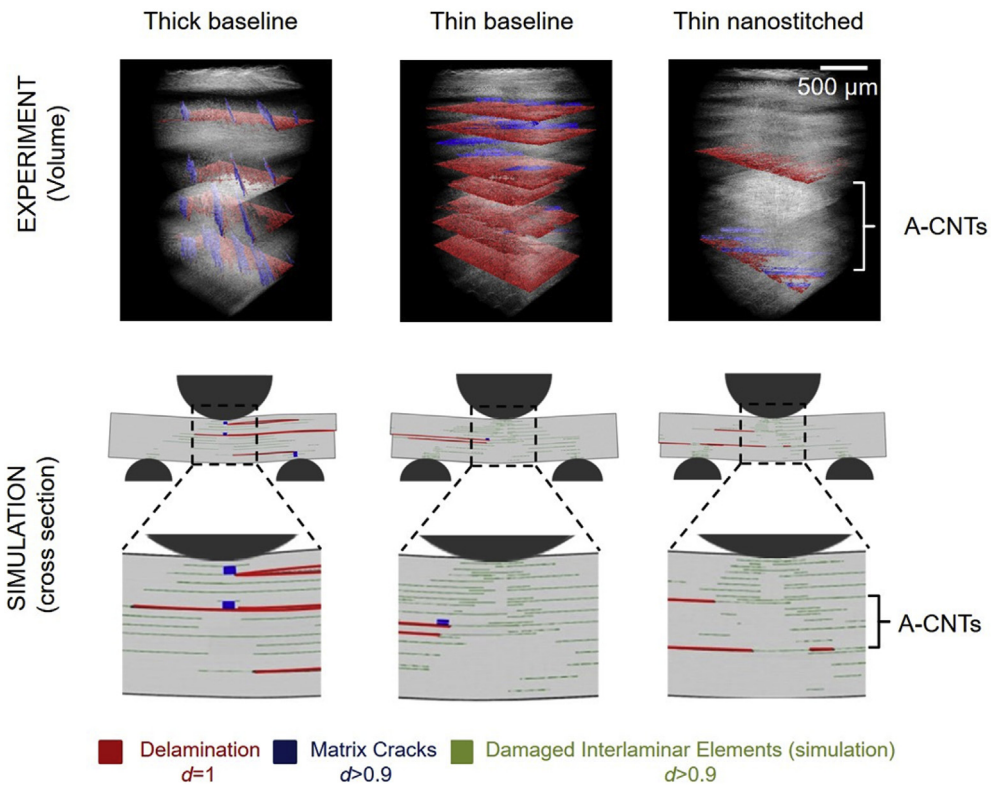

Fig. 4. 3D SRCT inspections of damage in *post mortem* coupons and model predictions (at 100% P_{max}): (top) *post mortem* SRCT 3D visualization of damage extent after SBS failure in Thick baseline, Thin baseline and Thin nanostitched, and (bottom) predicted damage at the specimen surface. Damage propagation is associated with a damage variable, d, with $d > 0.9$ for greatly damaged elements (see discussion in this section) and $d = 1$ for fully damaged elements. Colors represent: delamination (red), matrix cracking (blue), and damaged interlaminar elements (green). Note that fiber breaks exist in the images, concentrated at the contact zone, but are not shown/colored. (For interpretation of the references to color in this figure legend, the reader is referred to the Web version of this article.)

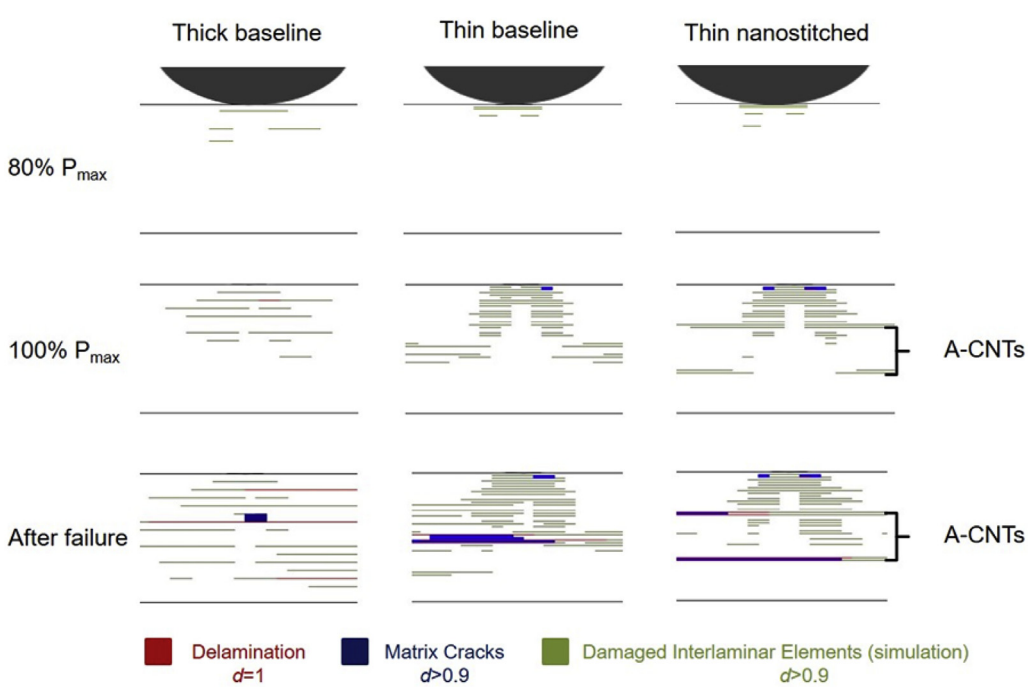

Fig. 5. Prediction of damage formation during SBS loading, shown as a projection of all internal (volumetric) damage integrated through the specimen width, for Thick baseline, Thin baseline, and Thin nanostitched laminates at (top to bottom) loadings of 80% P_{max}, immediately before failure (100% P_{max}), and after failure (~50% drop in load from P_{max}). Damage propagation is associated with a damage variable, d, with $d > 0.9$ for greatly damaged elements (see discussion in this section) and $d = 1$ for fully damaged elements. Colors represent: delamination (red), matrix cracking (blue), and damaged interlaminar elements (green). Only the region directly under the loading nose is shown. A 15% increase in fracture toughness values for the nanostitched interfaces is used as discussed in Section S3. (For interpretation of the references to color in this figure legend, the reader is referred to the Web version of this article.)

variable d is higher than 0.9 (see discussion in Section 2.5) are shown, for the sake of simplicity.

There is no damage at 80% of P_{max}, apart from that due to high compressive and shear stresses under the loading nose. Just before failure at 100% of P_{max}, the Thick and Thin baseline laminates show several partial damage at the interlaminar region, although ultimate failure is not yet reached. The Thin nanostitched configuration shows reduced interlaminar damage extent in the A-CNT region. This clear observation in the SRCT data is used as a criterion to select the value of 15% enhanced fracture toughness for modeling of the nanostitched interfaces (see discussion and supporting analyses in Section S3). This follows our observations in Fig. 4 and the hypothesis that the increased number of interfaces in the Thin baseline are prone to early failure (vs. the Thick baseline) as shown by the multiple damaged elements reported in the model. After failure (load drops to ~50% of P_{max}), the damage extent is increased in all configurations, with multiple interlaminar cracks and damage in the Thick baseline and Thin baseline that are largely absent in the Thin nanostitched configuration.

4. Conclusions and recommendations

We have reported the successful manufacture of thin-ply laminated advanced composites with aligned carbon nanotube nanostitching at ply interfaces and compared the mechanical performance in short beam shear strength testing for four laminate configurations, to compare thin and standard thickness plies, as well as nanostitching of both. The A-CNTs were transferred via a transfer printing technique without affecting the overall laminate thickness; however, a 50% increase in the interlaminar region thickness did result. Improvement of ILSS by 10% in Thin and an additional 5% increase in Thin nanostitched is noted over the Thick (baseline) laminates. SRCT observations reveal the suppression of large matrix-dominated cracks in Thin laminates, as well as the suppression of delamination in the nanostitched zone, vs. the baseline Thick (standard thickness) laminates. These findings were substantiated by progressive damage modeling results utilizing a 15% increase in Modes I and II interlaminar fracture toughness due to the A-CNTs. This work pioneers the investigation of synergies from two promising composite laminate technologies and gives fundamental insights into the damage progression and how it is affected by each technology separately, and together. Further investigation will focus on A-CNT height to establish structure-property relations towards enhancing these effects for increased SBS strength. Future work will undertake developing full predictive damage models utilizing cohesive zone laws measured for the A-CNT nanostitched laminates, as well as investigate other loading configurations, such as compression-after-impact (CAI), off-angle ply laminate bending, and open hole compression (OHC), that are known to be strongly influenced by delaminations, a mode of failure that thin-ply laminates are particularly susceptible to given the increased number of ply interfaces.

Acknowledgments

This work was supported by National Funds through FCT – Fundação para Ciência e a Tecnologia in the scope of project MITP-TB/PFM/0005/2013, partially supported by the U.S. Office of Naval Research under grant/contract number N00014-13-1-0213, and by Airbus, Embraer, Lockheed Martin, Saab AB, Hexcel, Saertex, Toho Tenax, and ANSYS through MIT's Nano-Engineered Composite aerospace STructures (NECST) Consortium. This work made use of facilities supported in part by the U.S. Army Research Laboratory and the U.S. Army Research Office through the Institute for Soldier Nanotechnologies, under contract number W911NF-13-D-0001, the facilities at the U.S. Army Natick Solider R, D & E Center (NSRDEC), and was carried out in part through the use of MIT's Microsystems Technology Laboratories (MTL). The SRCT experiments were performed on beamline ID 19 at the European Synchrotron Radiation Facility (ESRF), Grenoble, France. This work was performed in part at the Center for Nanoscale Systems (CNS), a member of the National Nanotechnology Coordinated Infrastructure Network (NNCI), which is supported by the National Science Foundation under NSF award no. 1541959. CNS is a part of Harvard University. For the second author, this material is based upon work supported by the National Science Foundation Graduate Research Fellowship Program under Grant No. 1122374. Any opinions, findings, and conclusions or recommendations expressed in this material are those of the author(s) and do not necessarily reflect the views of the National Science Foundation. The third author would like to thank Fundação para a Ciência e a Tecnologia, grant SFRH/BD/115859/2016. The authors thank Mike Kinsella and Joe Spangler (Toho Tenax) for helpful technical discussions, and Alan Alahmad (MIT) for experimental assistance. We are grateful to Lukas Helfen and Elodie Boller at the ESRF for providing assistance in using beamline ID 19. All authors thank Dr. Itai Stein and the entire necstlab at MIT and lab members at μ-VIS X-Ray Imaging Center at University of Southampton for valuable discussion and input. The authors thank Toho Tenax for materials donation of the thin-ply prepreg material.

Appendix A. Supplementary data

Supplementary data related to this article can be found at https://doi.org/10.1016/j.compscitech.2018.01.007.

References

[1] G. Han, Z. Guan, Z. Ji, S. Du, Initial damage induced by thermal residual stress and microscopic failure analysis of carbon-fiber reinforced composite under shear loading, Compos. Interfac. 22 (2015) 315–329.
[2] N.J. Pagano, R.B. Pipes, The influence of stacking sequence on laminate strength, J. Compos. Mater. 1 (1971) 50–57.
[3] C.T. Herakovich, Influence of layer thickness on the strength of angle-ply laminates, J. Compos. Mater. 16 (1982) 216–227.
[4] K. Kawabe, S. Tomoda, Multi-filament split-yarn sheet and method and device for the manufacture thereof. Patent no. 6032342, USA, 2000.
[5] K. Kawabe, S. Tomoda, Method of producing a spread multi-filament bundle and an apparatus used in the same. Patent no. 7832068, USA, 2010.
[6] K. Kawabe, S. Tomoda, T.A. Matsuo, A pneumatic process for spreading reinforcing fiber tow, in: Proceedings of the 42nd International SAMPE USA, Anaheim, CA, USA, 4–8 May 1997, pp. 65–76.
[7] H. Sasayama, K. Kawabe, S. Tomoda, I. Ohsawa, K. Kageyama, N. Ogata, Effect of lamina thickness on first ply failure in multidirectionally laminated composites, in: Proceedings of the 8th Japan International SAMPE, Tokyo Big Sight, Japan, 18–21 November 2003, pp. 18–21.
[8] K. Kawabe, H. Sasayama, S. Tomoda, New carbon fiber tow-spread technology and applications to advanced composite materials, SAMPE J. 45 (2009) 6–17.
[9] R. Amacher, J. Cugnoni, J. Botsis, L. Sorensen, W. Smith, C. Dransfeld, Thin ply composites: experimental characterization and modeling of size-effects, Compos. Sci. Technol. 132 (2014) 101–121.
[10] B. Sihn, R. Kim, K. Kawabe, S. Tsai, Experimental studies of thin-ply laminated composites, Compos. Sci. Technol. 67 (2007) 996–1008.
[11] T. Yokozeki, Y. Aoki, T. Ogasawara, Experimental characterization of strength and damage resistance properties of thin-ply carbon fiber/toughened epoxy laminates, Compos. Struct. 82 (2008) 382–389.
[12] C. Furtado, A. Arteiro, G. Catalanotti, J. Xavier, P.P. Camanho, Selective ply-level hybridisation for improved notched response of composite laminates, Compos. Struct. 145 (2016) 1–14.
[13] A. Arteiro, G. Catalanotti, J. Xavier, P.P. Camanho, Notched response of non-crimp fabric thin-ply laminates, Compos. Sci. Technol. 79 (2008) 97–114.
[14] A. Faggiani, B.G. Falzon, Predicting low-velocity impact damage on a stiffened composite panel, Compos. Part A 41 (2010) 737–749.
[15] L. Tong, A.P. Mouritz, M.K. Bannister, L. Tong, A.P. Mouritz, M.K. Bannister, 3D Fibre Reinforced Polymer Composites, Elsevier Science, 2002.
[16] K.A. Dransfield, L.K. Jain, Y.-W. Mai, On the effects of stitching in CFRPs-I: mode I delamination toughness, Compos. Sci. Technol. 58 (1998) 815–827.
[17] A.P. Mouritz, K.H. Leong, I. Herszberg, A review of the effect of stitching on the in-plane mechanical properties of fibre-reinforced polymer composites, Compos. Part A 28 (1997) 979–991.
[18] L. Gorbatikh, B.L. Wardle, S.V. Lomov, Hierarchical lightweight materials for

structural applications, MRS Bull. 41 (2016) 672–677.
[19] F. Larsson, Damage tolerance of a stitched carbon/epoxy laminate, Compos. Part A 28 (1997) 923–934.
[20] I.K. Partridge, D.D.R. Cartié, Delamination resistant laminates by Z-Fiber pinning: Part I manufacture and fracture performance, Compos. Part A 36 (2005) 55–64.
[21] K.T. Tan, A. Yoshimura, N. Watanabe, Y. Iwahori, T. Ishikawa, Effect of stitch density and stitch thread thickness on damage progression and failure characteristics of stitched composites under out-of-plane loading, Compos. Sci. Technol. 74 (2013) 194–204.
[22] N.A. Siddiqui, R.S.C. Woo, J.-K. Kim, C.C.K. Leung, A. Munir, Mode I interlaminar fracture behavior and mechanical properties of CFRPs with nanoclay-filled epoxy matrix, Compos. Part A 38 (2007) 449–460.
[23] T. Yokozeki, Y. Iwahori, S. Ishiwata, K. Enomoto, Mechanical properties of CFRP laminates manufactured from unidirectional prepregs using CNT-dispersed epoxy, Compos. Part A 38 (2007) 2121–2130.
[24] B. Fiedler, F.H. Gojny, M.H.G. Wichmann, M.C.M. Nolte, K. Schulte, Fundamental aspects of nano-reinforced composites, Compos. Sci. Technol. 66 (2006) 3115–3125.
[25] R.J. Sager, P.J. Klein, D.C. Lagoudas, Q. Zhang, J. Liu, L. Dai, J.W. Baur, Effect of carbon nanotubes on the interfacial shear strength of T650 carbon fiber in an epoxy matrix, Compos. Sci. Technol. 69 (2009) 898–904.
[26] P.R. Thakre, D.C. Lagoudas, J.C. Riddick, T.S. Gates, S.J.V. Frankland, J.G. Ratcliffe, J. Zhu, E.V. Barrera, Investigation of the effect of single wall carbon nanotubes on interlaminar fracture toughness of woven carbon fiber-epoxy composites, J. Compos. Mater. 45 (2011) 1091–1107.
[27] M.F.L. de Volder, S.H. Tawfick, R.H. Baughman, A.J. Hart, Carbon nanotubes: present and future commercial applications, Science 339 (2013) 535–539.
[28] E.J. Garcia, B.L. Wardle, J. Hart, N. Yamamoto, A. Slocum, Fabrication and multifunctional properties of a hybrid laminate with aligned carbon nanotubes grown *in situ*, Compos. Sci. Technol. 68 (2008) 2034–2041.
[29] E.J. Garcia, B.L. Wardle, J. Hart, A. Slocum, Joining prepreg composite interfaces with aligned carbon nanotubes, Compos. Part A 39 (2008) 1065–1070.
[30] J. Blanco, E.J. Garcia, R. Guzmán de Villoria, B.L. Wardle, Limiting mechanisms in mode I interlaminar toughness of composites reinforced with aligned carbon nanotubes, J. Compos. Mater. 43 (2009) 825–842.
[31] R. Guzmán de Villoria, P. Hallander, L. Ydrefors, P. Nordin, B.L. Wardle, In-plane strength enhancement of laminated composites via aligned carbon nanotube interlaminar reinforcement, Compos. Sci. Technol. 133 (2016) 33–39.
[32] D. Lewis, B.L. Wardle, Interlaminar shear strength investigation of aligned carbon nanotube-reinforced prepreg composite interfaces, in: AIAA SciTech 2015, Kissimmee, Florida, 5–9 January 2015.
[33] ASTM D2344, Standard test method for short-beam strength of polymer matrix composite materials and their laminates.
[34] E. Kalfon-Cohen, J. Orr, P. Skatis, L. Li, E. Shuter, D.J. Lewis, B.L. Wardle, Structure-process-property study of aligned carbon nanotube reinforcement height on interlaminar morphology in woven carbon fiber prepreg laminates, in: AIAA SciTech 2016, San Diego, California, 4–8 January 2016.
[35] P. Maimí, P.P. Camanho, J.A. Mayugo, C.G. Dávila, A continuum damage model for composite laminates: Part I – constitutive model, Mech. Mater. 39 (2007) 897–908.
[36] P. Maimí, P.P. Camanho, J.A. Mayugo, C.G. Dávila, A continuum damage model for composite laminates: Part II – computational implementation and validation, Mech. Mater. 39 (2007) 909–919.
[37] P. Maimí, Modelización constitutiva y computacional del daño y la fractura de materiales compuestos, Universitat de Girona, 2007.
[38] Dassault Systèmes, ABAQUS User's Manual, 2011.
[39] P.P. Camanho, C.G. Dávila, S.T. Pinho, L. Iannucci, P. Robinson, Prediction of in situ strengths and matrix cracking in composites under transverse tension and in-plane shear, Compos. Part A 37 (2006) 165–179.
[40] A. Turon, P.P. Camanho, J. Costa, An engineering solution for mesh size effects in the simulation of delamination using cohesive zone models, Eng. Fract. Mech. 74 (2007) 1665–1682.
[41] A. Turon, P.P. Camanho, J. Costa, J. Renart, Accurate simulation of delamination growth under mixed-mode loading using cohesive elements: definition of interlaminar strengths and elastic stiffness, Compos. Struct. 92 (2010) 1857–1864.
[42] X. Ni, E. Kalfon-Cohen, C. Furtado, R. Kopp, N.K. Fritz, A. Arteiro, G.A. Valdes, G. Borstnar, M.N. Mavrogordato, S.M. Spearing, P.P. Camanho, B.L. Wardle, Interlaminar reinforcement of carbon fiber composites using aligned carbon nanotubes, in: 21st ICCM, Xi'an, China, August 20–25th 2017.
[43] F. Abali, A. Pora, K. Shivakumar, Modified short beam shear test for measurement of interlaminar shear strength of composites, J. Compos. Mater. 37 (2003) 453–464.
[44] H. Saito, H. Takeuchi, I. Kimpara, A study of crack suppression mechanism of thin-ply carbon-fiber-reinforced polymer laminate with mesoscopic numerical simulation, J. Compos. Mater. 48 (2014) 2085–2096.

Electronic Supplementary Information:

Synergetic Effects of Thin Plies and Aligned Carbon Nanotube Interlaminar Reinforcement in Composite Laminates

Estelle Kalfon-Cohen[1*], Reed Kopp[1], Carolina Furtado[1,3,4], Xinchen Ni[2], Albertino Arteiro[3,4], Gregor Borstnar[5], Mark N. Mavrogordato[5], Ian. Sinclair[5], S. Mark Spearing[5], Pedro P. Camanho[3,4], and Brian L. Wardle[1]

[1] Department of Aeronautics and Astronautics, Massachusetts Institute of Technology,77 Massachusetts Avenue, Cambridge, MA 02139 USA
[2] Department of Mechanical Engineering, Massachusetts Institute of Technology, 77 Massachusetts Avenue, Cambridge, MA 02139 USA
[3] DEMec, Faculdade de Engenharia da Universidade do Porto, Rua Dr. Roberto Frias, s/n, 4200-465 Porto, Portugal
[4] INEGI, Instituto de Ciência e Inovação em Engenharia Mecânica e Engenharia Industrial, Rua Dr. Roberto Frias, 400, 4200-465 Porto, Portugal
[5] Faculty of Engineering and the Environment, University of Southampton, Highfield, Southampton, SO17 1BJ, UK

S1. Inspection of the interlaminar regions

Cross-sections of an A-CNT forest transferred on uncured prepreg are presented in Fig. S1A. The SEM images confirm that the alignment is maintained during the transfer process, preserving the original ~20μm height. Moreover, the micrograph in Fig. S1A (a) reveals that the forest does not experience any compression or crushing before curing. The transferred A-CNT nanostitch is weakly attached to the prepreg and no evidence of epoxy resin infiltration prior to cure is observed. This observation supports prior work with standard thickness prepreg that also observed that the CNT nanostitch is fully wetted by the resin and compressed during the autoclave cure.

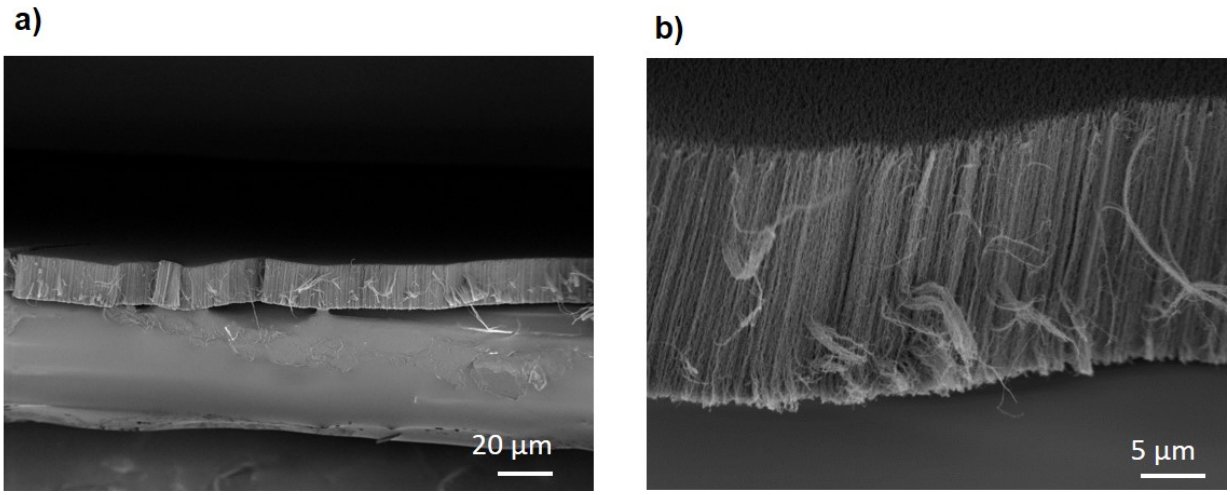

Fig. S1A: Scanning electron micrographs of A-CNT forest after transfer at two magnifications.

Thick baseline and nanostitched laminate cross-sections are presented in Fig. S1B. We can identify the three consecutive plies used to make the effective (via ply blocking) Thick laminate. Each ply within the block has identical fiber orientation forming ply blocks of ~160 µm. In Thick nanostitched, the A-CNTs are visible in the interlaminar region between two ply blocks (Fig S1B(b)) as the continuous light grey thick line. The micrograph reveals that the A-CNTs were effectively transferred onto the prepreg, properly filling the interlaminar resin rich area. Furthermore, the A-CNTs effectively bridge the two plies and penetrate the first row of microfibers as also observed for the Thin configurations.

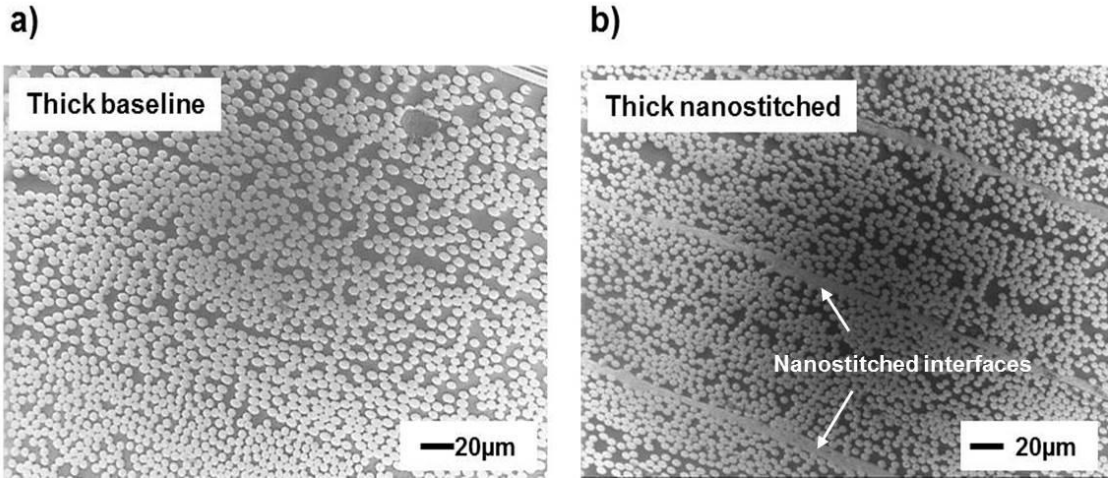

Fig. S1B: Scanning electron micrographs of Thick laminate cross-sections: (a) Thick baseline and (b) Thick nanostitched.

It should be noted that accurate measurement of the interlaminar thickness is difficult due to the irregularity of the interlaminar region, and therefore requires significant sampling. Hence, the interlaminar thickness for each laminate configuration was calculated from at least 10 measurements on each interface. Fig S1C shows representative low-resolution SEMs of Thin baseline and Thin nanostitched laminate cross-sections, showing large variations in the interlaminar thickness.

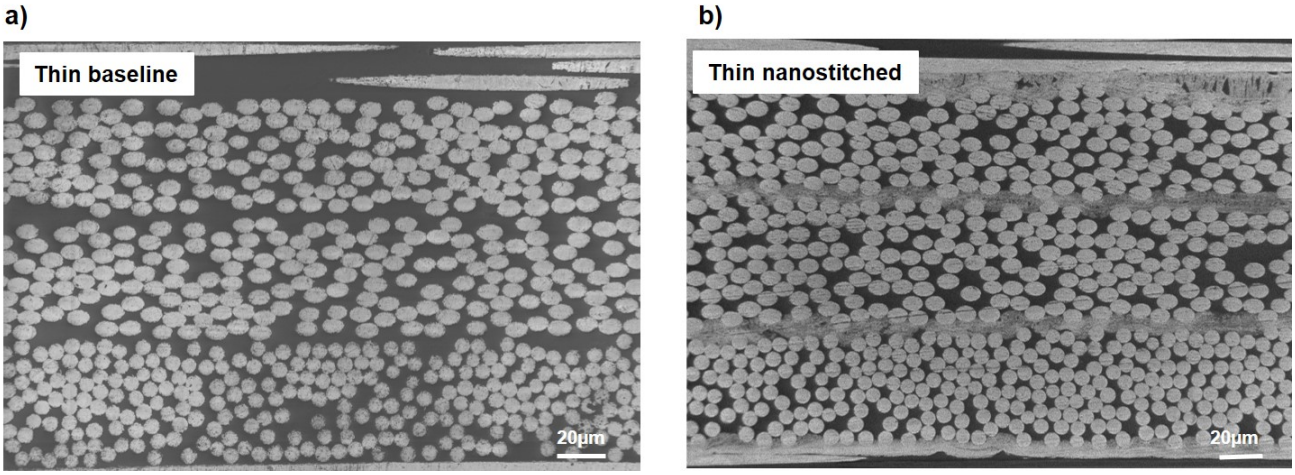

Fig. S1C: Scanning electron micrographs of representative interlaminar regions: (a) Thin baseline and (b) Thin nanostitched.

S2. Details of progressive damage finite element modeling

As explained in Section 2.5, intralaminar damage is simulated using the continuum damage model proposed by Maimí et al. [1-3] and interlaminar damage was simulated using the cohesive zone model implemented in ABAQUS [4]. The intralaminar model was developed to predict the onset and accumulation of intralaminar damage mechanisms (matrix cracking and fiber fracture) in laminated composites [1-3]. The continuum damage model was defined in the framework of the thermodynamics of irreversible processes. Generally speaking, the formulation of the continuum damage models starts by the definition of a potential (the complementary free energy density) as a function of a damage variable d, which is the basis for establishing the relation between the stress and the strain tensors. More details on the continuum damage model can be found in Refs. [1-3]. Regarding the simulation of interlaminar damage, the quadratic nominal stress criterion [4] and the Benzeggagh-Kenane fracture criterion [5] were used for damage initiation and damage propagation, respectively.

As described in Section 2.5, the short beam shear model includes two lower supports, a loading nose, and the laminate. The lower supports are clamped on the lower end and a smooth step with an amplitude of 1 mm is applied to the upper end of the loading nose. The mesh and boundary conditions used to simulate the short beam shear test are shown in Fig. S2.

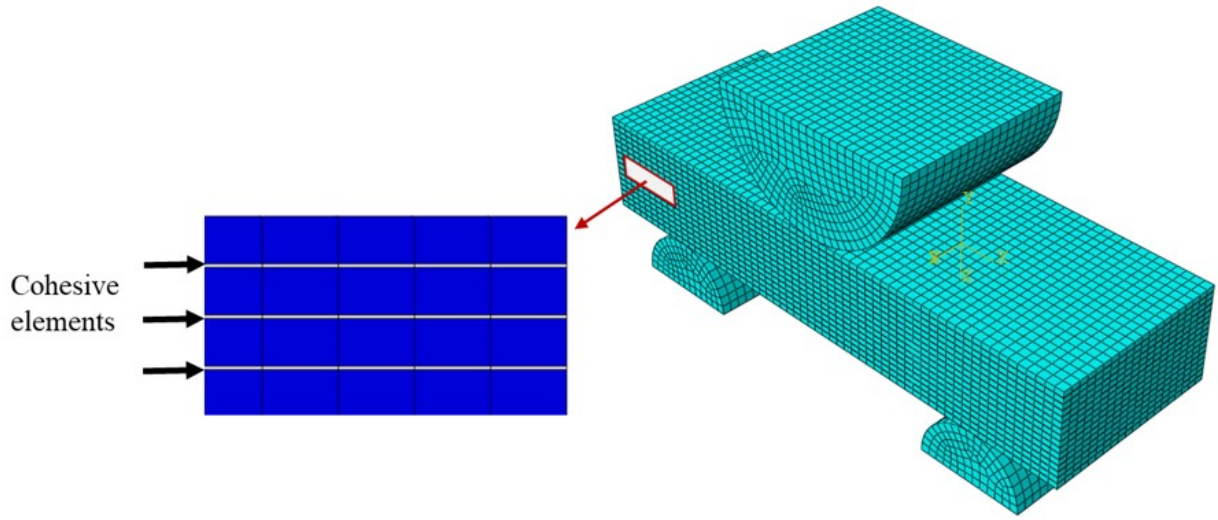

Fig. S2: Mesh and boundary condition used in the FEA model, with inset showing cohesive elements at ply interfaces.

S3. Numerical procedure for the determination of toughness enhancement factor in nanostitched laminates

Since most of the material properties needed to simulate intralaminar and interlaminar damage are unknown for the HTS40/Q-1112 carbon/epoxy material system, approximations as described in the main text are made. For the unknown properties, we used IM7/8552 (Hexcel) as a proxy system to complete the missing inputs. The most relevant ply properties used are presented in Table S3A. Note that the in-plane shear, transverse tensile, and transverse compressive strengths were calculated as a function of the ply thickness and ply position in the laminate following Ref. [9] and are therefore different for the Thin and Thick configurations. Following the notation in Ref. [9], "*inner plies"* are plies embedded in the laminate and "*outer plies*" are the 0º plies on the surface of the laminate. In the simulations of the unreinforced samples (Thick baseline and Thin

baseline) the fracture toughness of the elements in every interface is the same. However, since the middle fifteen interfaces are reinforced in the nanostitched samples, the fracture toughness of the elements on those interfaces is increased (see Table S3B). While the toughening factor induced by the presence of the A-CNTs is unknown, four enhancement factors are considered: 5%, 10%, 15%, and 20%.

The experimental and numerical interlaminar shear strengths obtained are compared in Table S3C. The load displacement curves obtained are linear up to failure. Note that, for the thin-ply samples, the errors obtained are higher than those obtained for the conventional grade/thickness Thick laminate (~4% vs. 10%). This may be attributed to the thinpreg *in-situ* strength effect, and these properties are not yet determined for the HTS40/Q-1112 material system. The interlaminar toughness enhancement factor was determined by comparing the experimental and numerical damage extents after failure for the Thin nanostitched configuration. We found that an increase of the fracture toughness of the A-CNT reinforced interfaces in the range of 10-15% is enough to shift the damage away from the center A-CNT region as observed experimentally, indicating that the nanostitch improves the fracture toughness by a factor of 1.10-1.15 as simulated in Fig S3, *i.e.,* the suppression of delaminations is used as a criterion to evaluate the appropriate percent increase. Values of the fracture toughness higher than 15% also result in the same behavior: interlaminar damage shifts away from the reinforced interfaces to the first non-reinforced interfaces; however, with a higher than 15% increase in the interlaminar fracture toughness, interlaminar and intralaminar damage is completely suppressed which is not observed experimentally. Although further work on Mode I and Mode II fracture toughness in nanostitched Toho Tenax HTS40/Q-1112 is required to confirm the model predictions, the similarities in the model results and damage profile and extent observed experimentally by SRCT suggest a 15% increase in G_{Ic} and G_{IIc} for

the present material is appropriate. For this reason, the numerical results for Thin nanostitched (+15% increase in fracture toughness is assumed) are presented with more detail in the paper, particularly in Figs. 4 and 5.

Table S3A: Relevant material properties used to simulate ply behavior of the HTS40/Q-1112.

Elastic Properties		
Long. Young's Modulus[1]	E_1	9.8 GPa
Trans. Young's Modulus[2]	E_2	6.0 GPa
Poisson Coefficient[2]	ν_{12}	0.32
Shear Modulus[2]	G_{12}	3.4 GPa
Fracture Toughness		
Long. Tension[3]	G_{XT}	133 kJ/m^2
Long. Comp.[3]	G_{XC}	60 kJ/m^2
Trans. Tension[4]	G_{Ic}	0.28 kJ/m^2
In-plane Shear[4]	G_{IIc}	0.79 kJ/m^2

Ply Strengths		
Long. Tension[1]	X^T	1471 MPa
Long. Comp.[5]	X^C	980 MPa
Inner 54 µm ply		
Trans. Tension[6]	Y^T	195 MPa
Trans. Comp.[6]	Y^C	310 MPa
In-plane Shear[6]	S^L	102 MPa
Outer 54 µm ply		
Trans. Tension[6]	Y^T	123 MPa
Trans. Comp.[6]	Y^C	253 MPa
In-plane Shear[6]	S^L	83 MPa
Inner 160 µm ply		
Trans. Tension [6]	Y^T	113 MPa
Trans. Comp.[6]	Y^C	310 MPa
In-plane Shear [6]	S^L	102 MPa
Outer 160 µm ply		
Trans. Tension[6]	Y^T	71 MPa
Trans. Comp.[6]	Y^C	253 MPa
In-plane Shear[6]	S^L	83 MPa

[1] Properties provided by Toho Tenax

[2] Typical values for carbon-epoxy material systems.

[3] These properties were assumed to be the properties measured for IM7/8552 carbon-epoxy material system reported in Refs. [6,7]

[4] These properties were assumed to be the properties measured for IM7/8552 carbon-epoxy material system reported in Ref. [8]

[5] The ratio X^T/X^C was assumed to be equal to around 1.5 as for other carbon-epoxy material systems

[6] *In-situ* properties calculated following Ref. [9]

Table S3B: Interlaminar properties used in short beam shear (SBS) modeling. The cohesive stresses were computed following Refs. [10-11]. The penalty stiffness used was 10^6 N/mm^3 as defined in Ref. [12].

Reference	Layup	Nanostitched interfaces	Assumed enhancement factor	G_{Ic} [kJ/m^2]	G_{IIc} [kJ/m^2]
Thick-baseline	$[(0_3/90_3/\pm45_3)]_{2s}$	None	-	0.28 [8]	0.79 [8]
Thin baseline	$[(0/90/\pm45)_6]_s$	None	-	0.28 [8]	0.79 [8]
Thin nanostitched 5%	$[(0/90/\pm45)_6]_s$	Middle 15 interfaces	5%	0.29	0.83
Thin nanostitched 10%	$[(0/90/\pm45)_6]_s$	Middle 15 interfaces	10%	0.30	0.87
Thin nanostitched 15%	$[(0/90/\pm45)_6]_s$	Middle 15 interfaces	15%	0.32	0.91
Thin nanostitched 20%	$[(0/90/\pm45)_6]_s$	Middle 15 interfaces	20%	0.34	0.95

Table S3C: Experimental and predicted ILSS of Thick baseline, Thin baseline, and Thin nanostitched laminates.

	Experimental ILSS (MPa)	Predicted ILSS (MPa)	Difference (%)
Thick baseline	69.90	67.35	-3.64
Thin baseline	76.90	69.90	-9.10
Thin nanostitched 5%	80.60	71.17	-11.70
Thin nanostitched 10%	80.60	71.77	-10.95
Thin nanostitched 15%	80.60	71.94	-10.74
Thin nanostitched 20%	80.60	72.50	-10.04

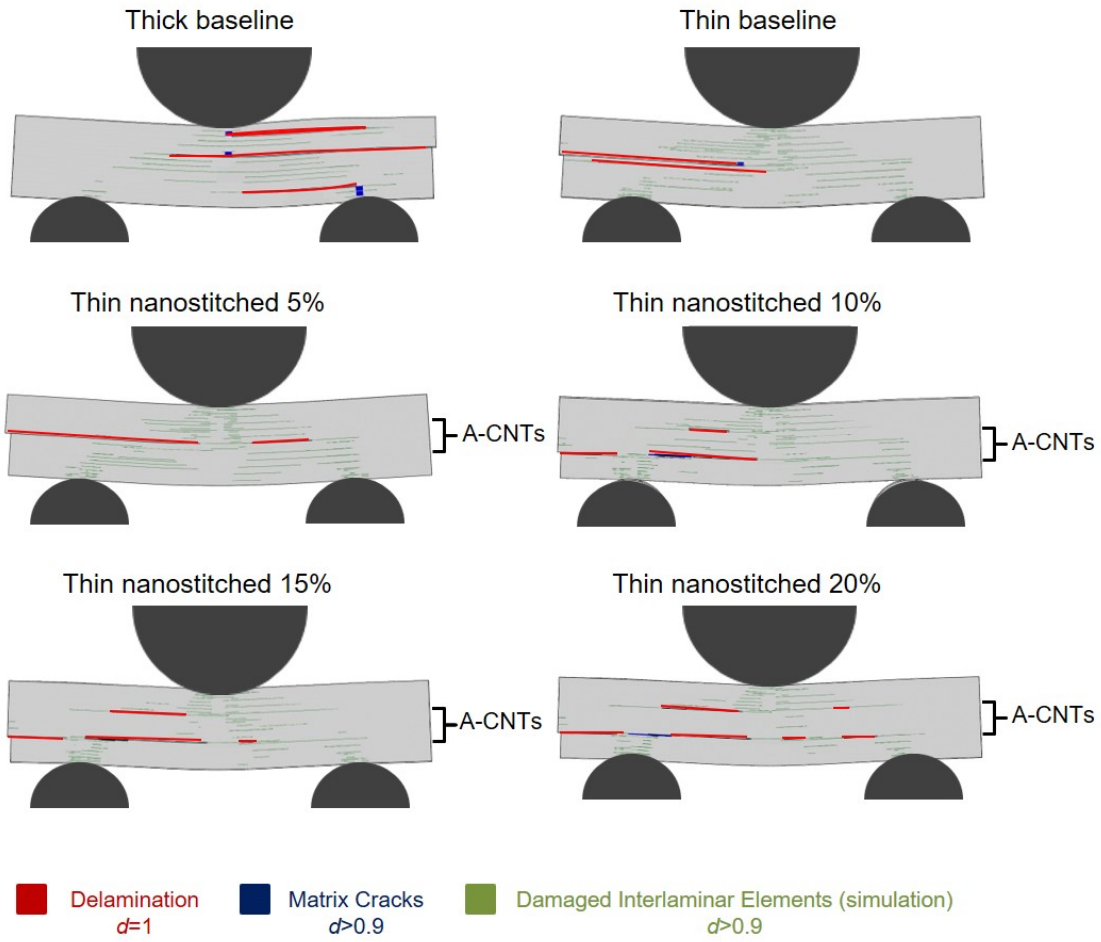

Fig. S3: Simulated interfacial damage (cross-sectional view) as a function of interlaminar toughness improvement at ~50% of ultimate load after failure (unloading SBS curve). The interlaminar toughness was increased from 0% (baseline) to 20% in Thin nanostitched. Damage propagation is associated with a damage variable, d, with d>0.9 for greatly damaged elements and d=1 for fully damaged elements. Colors represent: delamination (red), matrix cracking (blue), and damaged interlaminar elements (green).

Electronic Supplementary Information References

[1] P. Maimí, P.P. Camanho, J.A. Mayugo, C. G. Dávila, A continuum damage model for composite laminates: Part I – Constitutive model, Mech. Mater., 39 (2007) 897–908.

[2] P. Maimí, P.P. Camanho, J.A. Mayugo, and C. G. Dávila, A continuum damage model for composite laminates: Part II – Computational implementation and validation, Mech. Mater., 39 (2007) 909–919.

[3] P. Maimí, Modelización constitutiva y computacional del daño y la fractura de materiales compuestos, Universitat de Girona, 2007.

[4] Dassault Systèmes, ABAQUS User's Manual. 2011.

[5] M.L. Benzeggagh and M. Kenane, Measurement of mixed-mode delamination fracture toughness of unidirectional glass/epoxy composites with mixed-mode bending apparatus, Compos. Sci. Technol., 56 (1996) 439-449.

[6] G. Catalanotti, A. Arteiro, M. Hayati, P.P. Camanho, Determination of the mode I crack resistance curve of polymer composites using the size-effect law, Eng. Fract. Mech., 118 (2014) 49-65.

[7] G. Catalanotti, J. Xavier, P.P. Camanho, Measurement of the compressive crack resistance curve of composites using the size effect law. Compos Part A 56 (2014) 300- 307.

[8] M. Bessa, Meso-mechanical model of the structural integrity of advanced composite laminates. Master's thesis, Faculdade de Engenharia, Universidade do Porto, Porto, 2010.

[9] P.P. Camanho, C.G. Dávila, S.T. Pinho, L. Iannucci, P. Robinson, Prediction of in situ strengths and matrix cracking in composites under transverse tension and in-plane shear. Compos. Part A, 37 (2006) 165-179.

[10] A. Turon, P.P. Camanho, J. Costa, An engineering solution for mesh size effects in the simulation of delamination using cohesive zone models, Eng. Fract. Mech., 74 (2007) 1665–1682.

[11] A. Turon, P.P. Camanho, J. Costa, J. Renart, Accurate simulation of delamination growth under mixed-mode loading using cohesive elements: Definition of interlaminar strengths and elastic stiffness, Compos. Struct. 92 (2010) 1857–1864

[12] P.P. Camanho, C.G. Dávila, M.F. De Moura. Numerical simulation of mixed-mode progressive delamination in composite materials. J. Compos. Mater., 37 (2003) 1415-1438.